Fabrication and Performance of Solution-Based Micropatterned DNA Functionalized Carbon Nanotube Network as Humidity Sensors

Ambarish Paul, Baidurya Bhattacharya, and Tarun Kanti Bhattacharyya, *Member, IEEE*

***Abstract*—The paper describes a new technique of precise drop dispensing of deoxyribonucleic acid functionalized single walled carbon nanotube (DFC) solution by microfluidic cantilevers for use as resistance-type humidity sensors. Electrodes of different gap lengths $L = 10, 15, 20,$ and 25 μm were accurately bridged by DFC drops of desired diameter by regulating the relative humidity (RH) of the chamber, contact time t_c of the microcantilever type surface patterning tool touching the substrate and the UV/ozone exposure time t_{UV} of the substrate. Sensor performance, including sensitivity and dynamic response characteristics, is investigated in detail for $L = 25$ μm in the RH range of 20%–90%. The phenomenon of electric field assisted desorption of water molecules from the sensor surface is explained from the decrease in recovery time with the bias voltage. The device shows excellent dynamic repeatability and fairly good environmental stability over a period of one month.**

***Index Terms*—Biofunctionalization, carbon nanotubes (CNTs), deoxyribonucleic acid (DNA), drop dispensing, micropatterning.**

I. Introduction

A. Motivation

CARBON nanotubes (CNTs) have, over the last decade or so, emerged as an exciting platform for sensing technology [1]–[9]. Delocalized electrons on the surface of CNTs make them sensitive to any change in the local environment. However, uniform dispersion of CNTs in solution continues to be a challenge which has hindered advances in CNT-based sensors. Functionalizing CNTs with single-stranded DNA (ssDNA) appears promising in this regard [10], [11]. The ssDNA aids dispersion of nanotubes in water since its negatively charged phosphate backbone acts as a surfactant on CNT [12]. The ssDNA is immobilized on the surface of CNT via noncovalent van der Waals interactions [13], [14] and does not have significant influence on the conductance of individual nanotubes [15]. DNA functionalized CNTs (DFCs) have been used in chemical recognition of methanol, trimethylamine, propionic acid, 2,6 dinitrotoluene, dimethylephosphonate [16], and isopropanol [17]. The first ever use of DFC in humidity sensing was reported in our previous study [18] where a DFC network was used to create an FET-type humidity sensor.

B. State of the Art

System integration involving assembly of nanosized sensing materials in micron sized devices is crucial to (and still is a challenge in) the development and large-scale production of miniaturized sensors. Solution casting approaches such as tape casting [19], [20], screen printing [20], [21], spray deposition [20], [22], ink-jet printing [23]–[28], and drop dispensing [29], [30] are relatively easy and economical and thus are widely used in materials assembly. The first three techniques not only require temperatures in excess of 80 °C for curing causing permanent change in electronic properties of biomodified materials, but also form thick films of sensing material in the order of micrometers that result in deviation in transport properties. Ink-jet printing is relatively slow and the film thickness is higher than that in the drop dispensing technique owing to the repetitive casting process required to achieve the required percolation threshold [31]. The drop dispensing technique showed the promise of being used for low heat tolerant materials [32], but suffer from drop size control. Scientist have developed numerous solution dispensing technologies to solve this problem [33]. This technique also suffers from the problem of clogged orifice when the concentration of SWNTs in solution becomes high enough to form bundles. Covalent functionalization is extensively adopted to obtain highly dispersed solution of SWNT [34]. However, covalent functionalization of SWNT distorts the electronic property of the SWNTs [35] which brings about degradation in device performance. We propose an alternative technique of microcantilever-based drop dispensing which achieved the percolation threshold of the DNA functionalized CNT (DFC) network with a single drop cast.

C. Proposed Technique

Baba *et al*. [36] reported a strategy of micropatterning SWNT composites on Si-substrate using microfluidic cantilevers. We use this drop dispensing technique to drop-cast DFC solution and henceforth use it as a humidity sensor. We improve our syringe-based drop dispensing technique used in our previous study [18] to an advanced microcantilever-based drop dispens-

Manuscript received July 30, 2013; revised December 5, 2013; accepted January 21, 2014. Date of publication January 27, 2014; date of current version March 6, 2014. This work was partially supported by DST-ITPAR program and partially by BARC, Department of Atomic Energy, Government of India. The review of this paper was arranged by Associate Editor J. Li.

A. Paul is with the Advanced Technology Development Centre, Indian Institute of Technology Kharagpur, Kharagpur, West Bengal 721302, India (e-mail: ambarish@iitkgp.ac.in).

B. Bhattacharya is with the Department of Civil Engineering, Indian Institute of Technology Kharagpur, Kharagpur, West Bengal 721302, India (e-mail: baidurya@iitkgp.ac.in).

T. K. Bhattacharyya is with the Department of Electrical and Electronics Communications, Indian Institute of Technology Kharagpur, Kharagpur, West Bengal 721302, India (e-mail: tkb@ece.iitkgp.ernet.in).

Color versions of one or more of the figures in this paper are available online at http://ieeexplore.ieee.org.

Digital Object Identifier 10.1109/TNANO.2014.2302843

ing method which showed excellent accuracy and control over microcasting the DFC solution between Au electrodes. The technique achieves a drop cast of nanometer thickness and desired diameter that not only enhances dynamic recovery of the sensor but also prevents wastage of sensing material. The technique imparts consistency in film thickness and reduces stray signals which can evolve due to higher film thickness. This microcantilever-based technique of solution patterning is 30 times faster than ink-jet printing [7] as the required percolation threshold is achieved by microcasting the as-prepared solution between Au-electrodes only once. Our proposed technique requires suspension of isolated SWNTs in solution to prevent aggregation leading to clogging of the dispensing orifice. Isolation of individual SWNT was achieved by passivating its surface by noncovalently attaching ssDNA to it. The negatively charged phosphate backbone of the DNA wrapped around the SWNT not only isolates individual nanotubes in solution due to mutual electrostatic repulsion but also renders the SWNT network highly responsive so that any small physiochemical change in the neighborhood can be immediately sensed by change in conductivity of the network. The mutual repulsion among neighboring DFCs help them to maintain a highly dispersed state in the solution.

In this paper, we develop a humidity sensor by precise microcantilever-based drop dispensing of solution processed DFC between Au-electrodes of variable gaps. Electrodes of different gap lengths $L = 10$, 15, 20, and 25 μm were accurately bridged by DFC drops of desired diameter by regulating the relative humidity (RH) of the chamber, contact time t_c of the microcantilever type surface patterning tool (SPT) touching the substrate and the UV/ozone exposure time t_{UV} of the substrate. The maximum repeatability error in drop diameter for t_{UV} in the range 0–4 min was 14% and 9% for $t_c = 1$ and 2 s, respectively. The sensor performance parameters like sensitivity, response, and recovery times, dynamic repeatability reproducibility and environmental stability have be investigated. The evidence of electric field assisted desorption (EAD) of water molecules from the sensor bed is reported.

II. Experimental

A. Materials

The SWNTs, produced by CoMoCAT catalytic CVD process, were purchased from Sigma Aldrich, USA (Cat No. 704148). TEM investigation revealed the SWNT diameters to be in the range of 6–11 nm. The ssDNA sample constituting 41.9% G–C content and 58.1% A–T content in arbitrary sequence was purchased from Sigma Aldrich, USA (Cat No. D8899). The DNA strands have an average length of 587–831 base pairs and are best suited for functionalization applications. Tris-ethylene diamine tetraacetic acid (EDTA) buffer was purchased from Fluka Analytical BioUltra (Cat No. 93302–100 ml). The water used in the analysis and in solution was MilliQ quality (resistivity 18.2 MΩ-cm). The silicon wafers were n-doped with resistivity 4–20 Ωcm.

B. Synthesis of DFC

The DNA functionalized CNT (DFC) suspension in tris EDTA buffer solution was prepared with ssDNA and SWNT in the mass ratio 1:2 as follows. The ssDNA solution was prepared by adding 0.1 mg of ssDNA in 5 ml tris buffer solution and allowing the ssDNA to dissolve overnight in the sample mixer (HulaMixer from Life Technologies-Invitrogen, USA). 0.2 mg of SWNT was then added to the ssDNA solution and subjected to 4 h of alternate cycles of low intensity sonication for 30 min in an ice bath maintained at 0 °C and mixing for 30 min. This cycling allowed successful wrapping of ssDNA around SWNT going through the following sequence of steps—adsorption, disordered coating, partial ordering, and ordered coating [37]. The solution containing the DFC was filtered through Nuclepore track etch membrane (Whatman) of pore size 4 μm to eliminate the free standing ssDNA strands from the solution. The retentate was dissolved in tris buffer solution by sonicating the solution for 10 min until a uniform dispersion was obtained. The solution was subsequently centrifuged at 2000 r/min for 1 min to remove the large bundles of unmodified SWNTs which could not be dispersed during sonication. The supernatant solution was collected and preserved for drop dispensing on the fabricated electrodes. Since the free standing DNAs were removed from the solution as filtrate, the amount of unbound ssDNA could not be ascertained. The nucleobases of the ssDNA were bound to the surface of the SWNT by noncovalent π–π stacking interactions [38].

C. Fabrication of Au-Electrodes

For this paper, we used an n-doped Si-wafer with a thermally grown SiO_2 layer of thickness 250 nm as substrate. The Cr/Au layers of thickness 10 nm/150 nm were deposited on the SiO_2 substrate by thermal evaporation technique. Au-patterns of source and drain electrodes separated by gap lengths L of 10, 15, 20, and 25 μm were fabricated by conventional lithography technique using a UV exposure source of wavelength 405 nm. The width of the Au-electrodes measured by Dektak Profilometer Veeco150 were found to be 20 μm. Profilometer measurements showed that the fabricated gap length increased by 2 μm from the designed value due to Au-overetching and noncontact pattern transfer process.

D. Drop Size Control by Nano eNabler System

Micropatterning of DFC solution between Au-electrodes requires precise position and drop diameter control so that the DFC network just bridges the electrodes at a desired location thereby preventing wastage of sensing material. The DFC in tris-EDTA buffer was drop cast using Nano eNabler system (Bioforce Nanosciences, USA) having an SPT attachment in the form of microfluidic-based cantilevers of channel width 30 μm, as shown in Fig. 1(a). UV/ozone exposure was performed using UV/Ozone Procleaner (PC) (Bioforce Nanosciences, USA). Fig. 1(b) shows the dispensing of drops by SPT at RH 50% and $t_{\mathrm{UV}} = 2$ min for $t_c = 1$, 2, and 3 s.

The diameter of the DFC drop dispensed by this technique depends on the RH of the humidity chamber (HC) (Bioforce, USA), t_c, hydrophilicity of the substrate regulated by t_{UV}, and viscosity of the solution. The effect of viscosity on the drop diameter was not studied in this paper. The UV/Ozone exposure renders the substrate hydrophilic so that the DFC solution can

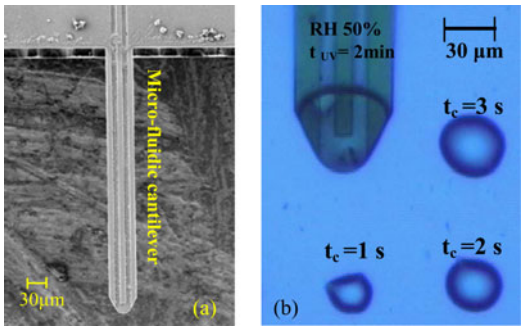

Fig. 1. (a) FESEM image of SPT. (b) Dispensed drops of DFC by SPT at RH 50% and $t_{\rm UV} = 2$ min for $t_c = 1$, 2, and 3 s.

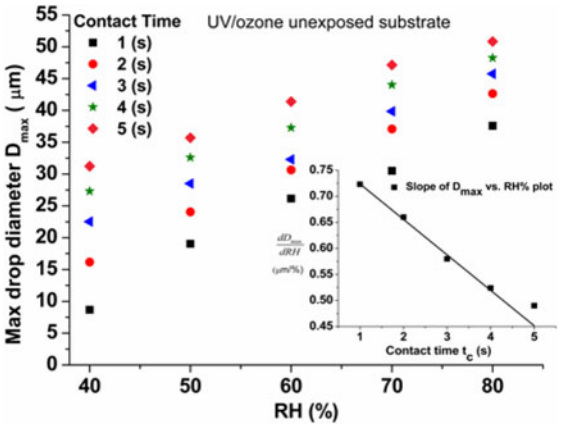

Fig. 2. Dependence of RH% on drop size for different contact times (t_c) for UV/ozone unexposed SiO_2 substrate.

be easily transferred to the substrate through capillary action. Optimal RH, t_c and $t_{\rm UV}$ is ascertained to achieve precise control over desired drop diameter.

Fig. 2 shows a linear relation of maximum drop diameter $D_{\max}$ with RH% in the range 40%–80% for different contact times (t_c) from 1–5 s when the substrate was not exposed to UV/ozone treatment. Compared to that for lower RH, drops of larger diameter are dispensed by the SPT under condition of higher RH.

$D_{\max}$ was also observed to increase almost linearly with t_c (see Fig. 3). Observations from the $D_{\max}$ versus t_c plot in Fig. 4, obtained at RH 50% for different UV/ozone exposure times $t_{\rm UV}$ in the range 0–4 min showed that the drop size can be controlled by UV ozone treatment of the SiO_2 substrate. Drop diameter, at RH 50%, can be varied in the range 14–28 μm and 26–38 μm with $t_c = 1$ and 2 s, respectively, by mere UV/ozone exposure of the substrate. Since $t_{\rm UV}$ can be conveniently and accurately fixed using a timer clock in PC, it serves as the most precise drop size control parameter in our experiment. Based on these observations, fabrication of devices in this paper was performed at $t_c = 1$ s for $L = 10$, 15, and 20 μm, and $t_c = 2$ s for 25 μm.

Fig. 5 shows the variation of $D_{\max}$ with $t_{\rm UV}$ for the two values of $t_c = 1$ and 2 s. $D_{\max}$ show linear behavior up to about $t_{\rm UV} = 2$–3 min beyond which $D_{\max}$ tends to saturate. The increase in hydrophilicity of the substrate with UV/ozone exposure causes the formation of temporary monolayer of free radicals which gets saturated after sufficient UV/ozone exposures. The error bars in the figure correspond to 10 drops for each $t_{\rm UV}$, t_c combination showing good repeatability (4%–14% for $t_c = 1$ s and 6%–9% for $t_c = 2$ s in the range of $t_{\rm UV} = 0$ to 4 min).

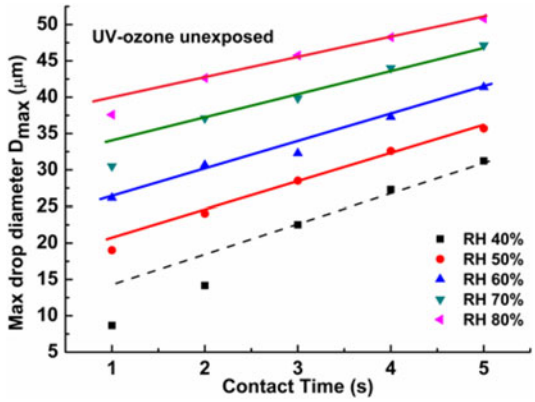

Fig. 3. Dependence of contact time t_c on drop size obtained for different RH% for UV/ozone unexposed SiO_2 substrate.

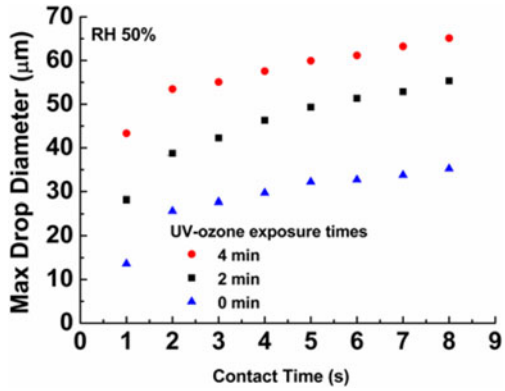

Fig. 4. $D_{\max}$ versus t_c plot for $t_{\rm UV} = 0$, 2, 4 min performed at RH 50%.

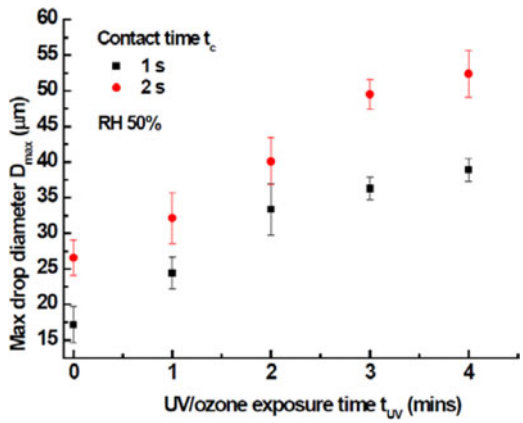

Fig. 5. Plot of $D_{\max}$ versus $t_{\rm UV}$ for contact times $t_c = 1$ and 2 s. Error was calculated from standard deviation of 10 data points about the mean current I.

Table I shows the drop casting parameters selected in this paper to bridge the desired electrode gap lengths L. Corresponding values of $D_{\max}$ (last column) account for Au etching loss of 1 μm and incorporate an overlap of 3 μm on either Au electrodes for each of the devices.

TABLE I
DESIRED D_{max} FOR DIFFERENT L

L(μm)	RH%	t_c (s)	t_{UV} (min)	Desired D_{max}±Err.
10	50	1	0	17.5±2.5
15	50	1	1	24.5±2.2
20	50	1	2	32.4±3.6
25	50	2	2	41.0±3.3

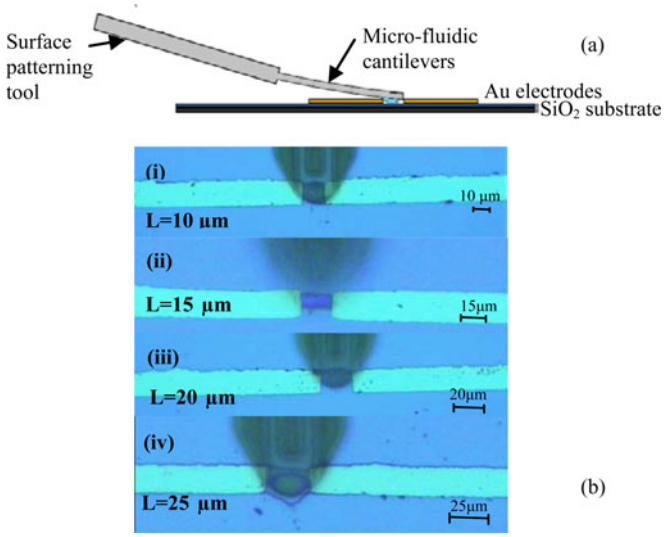

Fig. 6. (a) Side view of the dispensing process brought about by capillary action of the fluid. (b) Photographs of solution dispensing of DFC by SPT between device electrodes of (i) $L = 10$ μm, (ii) 15 μm, (iii) 20 μm, and (iv) 25 μm.

E. Micropatterning of DFC Solution

The SPT was turned hydrophilic by UV/ozone treatment for 40 min. Fig. 6(a) shows the schematic side view of the dispensing process between Au electrodes by SPT. DFC was drop dispensed on $L = 10$, 15, 20, and 25 μm, according to the protocol laid down in Table I and shown in Fig. 6(b) i–iv. The diameter and thickness of the DFC drop-cast between Au-electrodes for $L = 10$, 15, 20, and 25 μm were determined by 3-D surface scan using Dektak Profilometer Veeco150 as 15, 22, 27, and 35 μm, respectively. The 3-D profilometer image and the height profile for the case of $L = 25$ μm are shown in Fig. 7(a) and (b), respectively.

F. Device Characterization Setup

The experimental set-up for the electrical characterization of the as fabricated device is illustrated in Fig. 8. The device was mounted on the sample stage S and was connected to semiconductor parameter analyzer (4155C, Agilent Technologies) through a test box (16442A, Agilent Technologies). The HC included a humidifier F that fed a controlled amount of water vapor into it. The RH within HC depended on the volumetric ratio of moist air from F and dry N_2 from the gas inlet O. The RH was monitored by a commercial digital hygrometer (Model: Kusam Meco. 918, resolution 0.1 RH%, accuracy 2.5% of RH) kept within HC. Electrical measurements were performed after allowing the patterned DFC solution to dry up at 25 °C for 24 h.

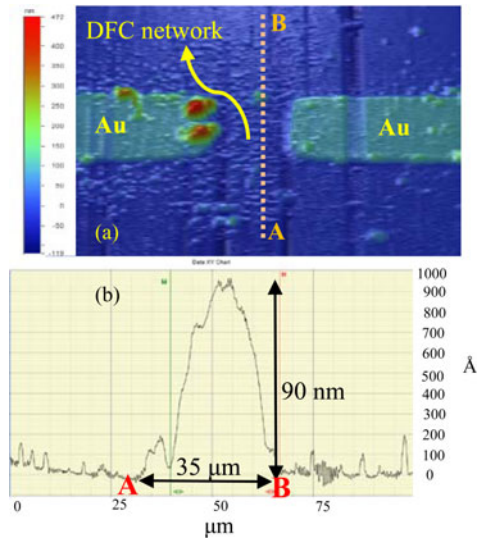

Fig. 7. (a) Dektak profilometer image of micropatterned device. (b) Height profile of the DFC network between A and B.

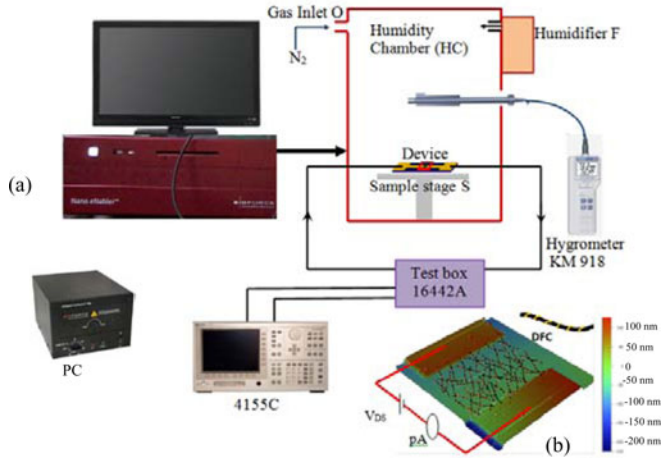

Fig. 8. (a) Schematic representation of the experimental test set-up and (b) circuit diagram.

The circuit diagram for the electrical characterization is shown in Fig. 8(b).

G. Electrical Characterization

Electrical measurements were conducted on as fabricated devices with $L = 10$, 15, 20, and 25 μm in the RH range 40%–80% at V_{DS} 2.5 V as shown in Fig. 9. The I versus RH calibration curve for device with $L = 10$ μm was found to be steeper than that for $L = 25$ μm. The experimental data for all the calibration curves were exponentially fitted as

$$I = \alpha e^{\beta \times \mathrm{RH}} - I_0 \tag{1}$$

where α, β, and I_0 are constants that depend on electrode gap length L and bias voltage V_{DS}. The constants for a fixed $V_{DS} = 2.5$ V are listed in Table II.

Fig. 9 also shows that the I–RH curves are nonlinear. Thus, the sensitivity S of the humidity sensor is obtained by differentiating

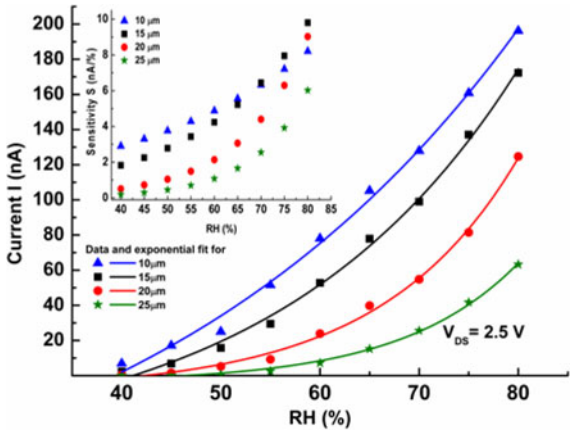

Fig. 9. I versus RH plot for devices with electrode gap $L = 10$, 15, 20, and 25 μm. (Inset) sensitivity S versus RH% plot for the same devices.

TABLE II
LIST OF CONSTANTS OF (1) AT DIFFERENT L

Constants	I_o	α	β	R^2
L (μm)	(nA)			
10	107.61	39.43	0.026	0.995
15	44.13	8.11	0.042	0.996
20	8.56	0.395	0.072	0.996
25	3.84	0.072	0.086	0.996

(1) as

$$S = \frac{dI}{d\mathrm{RH}} = \alpha\beta e^{\beta.\mathrm{RH}}. \tag{2}$$

The S versus RH% curve for all the four devices with $L = 10$, 15, 20, and 25 μm are plotted in Fig. 9(inset). Since S increases exponentially with RH% the device is more sensitive at higher RH than at a lower RH. The S for devices with $L = 15$, 20, and 25 μm were found higher than that for device with $L = 10$ μm for higher RH in the range 70%–80%, which may be attributed to lower sensing area for the latter device.

Although resistive chemical sensors with lower electrode gap enjoy higher sensitivities, SWNT–FET-based devices with higher channel length have higher ON/OFF ratio suited for switching applications [39]. Aimed at the development of DFC–FET with higher ON/OFF ratio we carry on our investigations for different sensor parameters with fabricated devices with $L = 25$ μm as discussed in the following section.

III. SENSOR PERFORMANCE

It was observed in our earlier study [18] that the conductance of the DFC network increases exponentially with increasing levels of RH, making DFC a potential sensing material for humidity sensor especially at higher RH. In this paper, we extend our investigation to obtain the calibration curves for wider range of bias voltage V_{DS} and find its optimum value. The section also addresses the influence of variation of bias voltage on the dynamic response of the humidity sensor. This paper investigates the repeatability and also focuses on its environmental stability of the device.

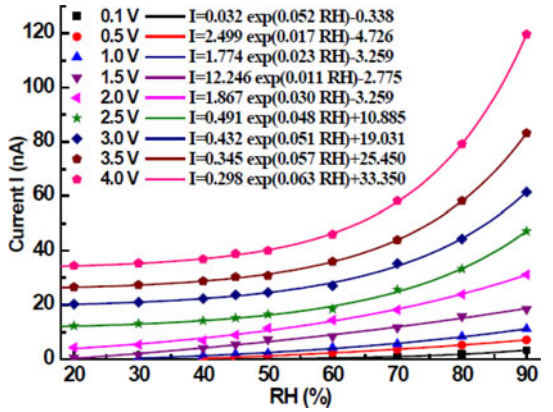

Fig. 10. Output signal current I versus RH plot at various bias voltages V_{DS}.

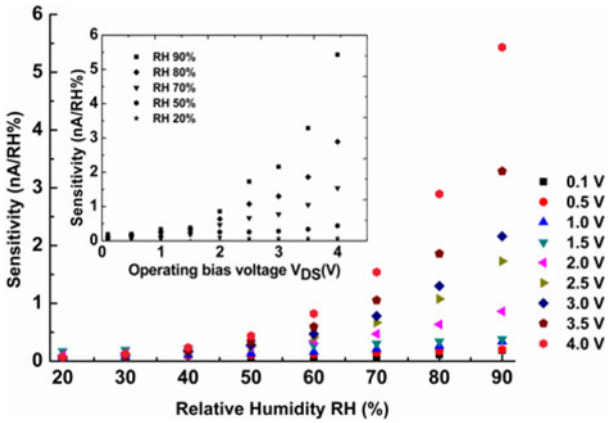

Fig. 11. Sensitivities of the DFC-based humidity sensor at different operating voltages and calculated from (2).

A. Calibration Curve

The I versus RH calibration of the device with $L = 25$ μm for bias voltage (V_{DS}) ranging from 0.1 to 4.0 V was performed under normal atmospheric pressure and at temperature 20 °C. For a fixed V_{DS}, current I was recorded in the RH range of 20%–90%. Condensation on the cooler HC wall prevented going above 90% RH. All calibration curves obtained for V_{DS} of 0.1–4.0 V show exponential rise in I with RH% as shown in Fig. 10 and were fitted in (1), where α, β, and I_0 listed in the plot are defined as constants for the calibration curve for a fixed $L = 25$ μm. The minimum recorded S/N ratio among all these curves was 17.40 (at RH 80% and V_{DS} 1.0 V).

B. Sensitivity

The sensitivity of the device with RH for V_{DS} from 0.1 to 4.0 V is shown in Fig. 11. Clearly the sensitivity increases exponentially with RH% for all V_{DS}. Fig. 11 (inset) shows the variation of sensitivity with V_{DS}. At a constant RH 70%, the sensitivity was 0.47 and 1.541 nA/RH% when the device was operated at 2.0 and 4.0 V, respectively. The device is best suited for applications where sensitivity is the primary requirement as in medical services, incubator, and spinning in textile industry [40].

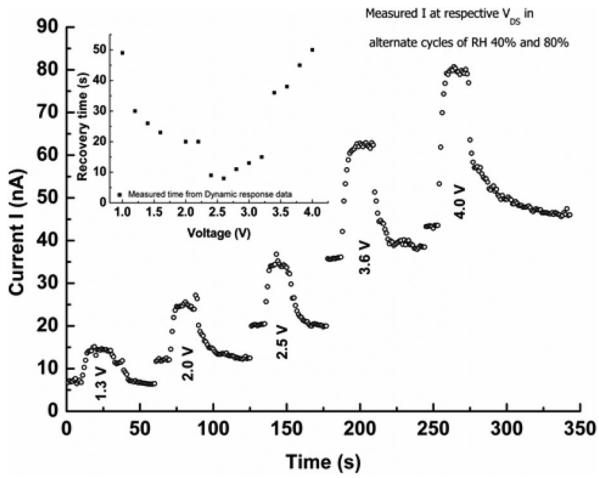

Fig. 12. Dynamic response of the device at different bias voltages of 1.3, 2.0, 2.5, 3.6, and 4.0 V showing the variation in recovery time. (Inset: plot of the recovery time versus bias voltage.)

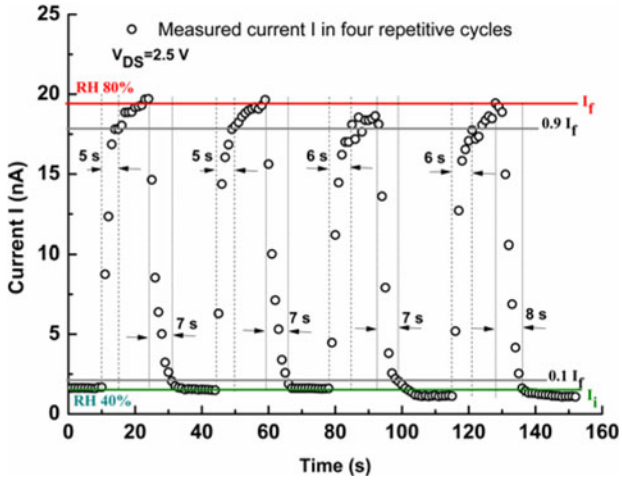

Fig. 13. Dynamic response of DFC-based humidity sensor operated at bias voltage of 2.5 V.

C. Dynamic Characteristics

The response and recovery times of a sensor are determined from its dynamic response characteristics. Fig. 12 shows the I versus time response of the device switched between RH 40% (initial state) and 80% (final state) at different bias voltages between 1.3 and 4.0 V. Response time of a sensor is the time required for the current to rise from the base line I_i (at RH 40%) to 90% of the finally settled current (I_f) corresponding to RH 80%. The recovery time is the time required for the current to fall below 10% of I_f. The response times for our device were observed to be fairly constant at 5 s for all operating $V_{\rm DS}$. Importantly, the recovery time was found to decrease with $V_{\rm DS}$ and showed a minimum of 7 s at $V_{\rm DS}$ 2.6 V (see Fig. 12 inset) signifying EAD of water molecules from the sensor bed.

The phenomena of EAD can be explained by the concept of orientation polarization between two interacting dipoles. At increased $V_{\rm DS}$, by the virtue of higher mutual potential energy Φ_{ij} of interacting molecular dipoles of water two neighboring dipoles are thrown into a nonequilibrium state when they tend to minimize their energy by avoiding the influence of the applied electric field *E.* The easiest possible way to evade the field is by the process of desorption following which the individual dipole moments of water can revert back to the randomly oriented equilibrium state of minimum Φ_{ij}.Thus, higher the state of polarization in DFC, more rapid is the rate of release of water molecules from its surface. Consequently, the recovery time strongly reduces with increase in $V_{\rm DS}$. The increase in recovery time at higher $V_{\rm DS}$ (>2.6 V) was due to entrapment of charged ions beneath the ultrathin layers of water which delays the recovery of the sensor to the initial lower RH state. Thus, dynamic characteristics of humidity sensors should be taken into consideration while selecting the optimal operating voltage.

D. Dynamic Repeatability

Repeatability is the ability of the sensor to produce the same output signal current under identical environmental and operating conditions. The repeatability of the device was studied at $V_{\rm DS} = 2.5$ V (so chosen to be close to the condition of minimum response and recovery times) by subjecting the device to alternate exposures of RH 40% and RH 80% for 10 s each for four identical cycles as shown in Fig. 13. There was insignificant negative baseline drift on subsequent repetitive measurement cycles which confirms that on exposure to higher RH, the increase in conductance was not governed by adsorption and desorption of water molecules, but solely dominated by charge transfer mechanism [18].

Repeatability error δ_r is defined as the ratio of the difference between output currents in two different calibrating cycles (ΔI_f) and the full scale output signal current (I_f) and is denoted by

$$\delta_r = \frac{\Delta I_f}{I_f} \times 100\%. \tag{3}$$

At RH 80%, δ_r was 5.5%.

E. Fabrication Reproducibility and Environmental Stability

Five devices were fabricated and developed under identical process flow and micropatterning technique. Reproducibility in calibration curves of fabricated devices in the RH range 20–80% were studied at $V_{\rm DS} = 2.5$ V as shown in Fig. 14. The minimum and maximum reproducibility error about the mean current I was found to be 5.8% and 27.14% at RH 30% and RH 65%, respectively. These variations in conductance are presumably due the presence of SWNTs of different chiralities in the sample material. Fabrication reproducibility can be increased by using SWNTs that do not widely vary in electronic properties, and realized through novel growth techniques [41].

The study of stability of the sensor against environmental exposure was carried over a period of 100 days. Electrical measurements were conducted in an interval of 10 days at temperature of 20 °C. The plot of the measured signal current I with time is shown for different RH levels from 40% to 90% RH in Fig. 14 (inset). The percentage variation in output signal current

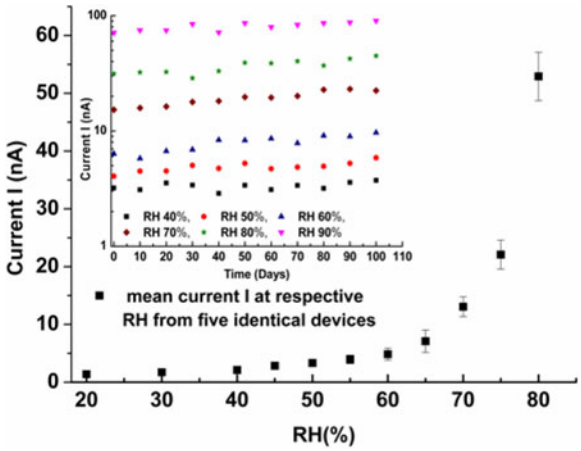

Fig. 14. Fabrication reproducibility of the device studied through calibration curves of five identical devices. (Inset) variations in output current I with time at different RH%.

TABLE III
STUDY OF ENVIRONMENT STABILITY OF THE SENSOR

RH (%)	Percentage Variation in Output Current I after		
	30 Days	60 days	90 days
40	2.81	3.13	11.9
50	3.37	5.62	17.8
60	1.91	9.69	14.4
70	3.25	19.6	41.7
80	2.23	23.	35.0
90	4.91	11.64	22.6

is obtained from the following relation:

$$\frac{\Delta I(t)}{I_0} = \frac{\text{measured current at time } t}{\text{initial measured current}} \times 100\% \qquad (4)$$

and is listed in Table III at 30, 60, and 90 days. The device shows good environmental stability up to one month (less than 5% variation) and is consistent with results obtained for devices developed with nanomaterials [42].

IV. CONCLUSION

We presented a technique of precisely micropatterning solution processed ssDNA functionalized CNT (DFC) network between different Au electrode gap lengths by microcantilever-based SPT and using the device as humidity sensor. The functionalization of SWNT by ssDNA not only debundles the nanotubes by electrostatic repulsion but also increases the solubility of DFC in aqueous solution and prevents accumulation in the microfluidic channel. As the microcantilever type drop casting technique attains the required percolation threshold in a single drop cast, the fabrication time is highly reduced. The technique not only dispenses DFC solution on a desired location but also possesses precise control over drop size producing minimal wastage of sensing material. Different electrode gap lengths were accurately bridged by DFC drops of desired diameters by regulating the RH of the chamber, contact time t_c of the microcantilever type SPT touching the substrate and the UV/ozone exposure time t_{UV} of the substrate. The technique achieved a good repeatability in drop size with an error of 4%–14% for $t_c = 1$ s and 6%–9% for $t_c = 2$ s in the range of $t_{\mathrm{UV}} = 0$ to 4 min.

The DFC-based humidity sensor works on the principle of variation of conductance of DFC network on exposure to water molecules. The sensor was found highly sensitive to humidity especially at high RH and that the sensitivity S of the device increases with bias voltage. Sensitivity S was also found to increase with electrode gap length L. However, at high RH, the devices with $L = 15$, 20, and 25 μm showed higher S than for $L = 10$ μm, which is attributed to higher sensing areas in the former cases.

EAD of water molecules from the sensor bed is explained from the decrease in recovery time from 48 to 7 s when bias voltage was increased from 1.3 to 2.6 V. EAD is attributed to the (nearly) parallel orientation of molecular dipoles along the external field E which raises the potential energy of interacting dipoles, allowing rapid release of water molecules from the surface of the DFC. The increase in recovery time at higher V_{DS} (> 2.6 V) was due to entrapment of charged ions beneath the ultrathin layers of water. After one month the DFC shows an error within 5% due to environmental degradation. The devices showed good dynamic repeatability over consecutive measurement cycles with an error of 5.5% at RH 80%. As the sample material contains metallic as well as semiconducting SWNTs of different chiralities the fabrication reproducibility suffers a maximum error of 27.14%. The technique is most suitable for the development of solution processed biofunctionalized SWNT-based sensors as it does not require drying of sensing material after drop casting.

REFERENCES

[1] S. Chopra, K. McGuire, N. Gothard, A. M. Rao, and A. Pham, "Selective gas detection using a carbon nanotube sensor," *Appl. Phys. Lett.*, vol. 83, pp. 2280–2282, 2003.
[2] J. Li, Y. Lu, Q. Ye, M. Cinke, J. Han, and M. Meyyappan, "Carbon nanotube sensors for gas and organic vapor detection," *Nano Lett.*, vol. 3, pp. 929–933, Jun. 2003.
[3] Y. D. Lee, W.-S. Cho, S.-I. Moon, Y.-H. Lee, J. K. Kim, S. Nahm, and B.-K. Ju, "Gas sensing properties of printed multiwalled carbon nanotubes using the field emission effect," *Chem. Phys. Lett.*, vol. 433, pp. 105–109, 2006.
[4] J. Suehiro, H. Imakiire, S.-i. Hidaka, W. Ding, G. Zhou, K. Imasaka, and M. Hara, "Schottky-type response of carbon nanotube NO_2 gas sensor fabricated onto aluminum electrodes by dielectrophoresis," *Sens. Actuators B*, vol. 114, pp. 943–949, 2006.
[5] C. S. Huang, B. R. Huang, Y. H. Jang, M. S. Tsai, and C. Y. Yeh, "Three-terminal CNTs gas sensor for N_2 detection," *Diamond Related Mater.*, vol. 14, pp. 1872–1875, 2005.
[6] M. Tabib-Azar and Y. Xie, "Sensitive NH_3 OH and HCl gas sensors using self-aligned and self-welded multiwalled carbon nanotubes," *IEEE Sens. J.*, vol. 7, no. 10, pp. 1435–1439, Oct. 2007.
[7] P. Teerapanich, M. T. Z. Myint, C. M. Joseph, G. L. Hornyak, and J. Dutta, "Development and improvement of carbon nanotube-based ammonia gas sensors using ink-jet printed interdigitated electrodes," *IEEE Trans. Nanotechnol.*, vol. 12, no. 2, pp. 255–262, Mar. 2013.
[8] M. Ouyang, W. J. Li, P. H. W. Leong, and K. W. Wong, "Improving carbon nanotubes sensor time response and responsivity using constant-power activation," *IEEE Trans. Nanotechnol.*, vol. 11, no. 3, pp. 624–632, May 2012.
[9] J. Zhang, N. Xi, H. Chen, K. W. C. Lai, G. Li, and U. C. Wejinya, "Design, manufacturing, and testing of single-carbon-nanotube-based infrared sensors," *IEEE Trans. Nanotechnol.*, vol. 8, no. 2, pp. 245–251, Mar. 2009.
[10] M. Zheng, A. Jagota, E. D. Semke, B. A. Diner, R. S. Mclean, S. R. Lustig, R. E. Richardson, and N. G. Tassi, "DNA-assisted dispersion and separation of carbon nanotubes," *Nature Mater.*, vol. 2, pp. 338–342, 2003.
[11] A. Paul and B. Bhattacharya, "DNA functionalized carbon nanotubes for nonbiological applications," *Mater. Manuf. Processes*, vol. 25, pp. 891–908, 2010.

[12] M. Zheng, A. Jagota, M. S. Strano, A. P. Santos, P. Barone, S. G. Chou, B. A. Diner, M. S. Dresselhaus, R. S. McLean, G. B. Onoa, G. G. Samsonidze, E. D. Semke, M. Usrey, and D. J. Walls, "Structure-based carbon nanotube sorting by sequence-dependent DNA assembly," *Science*, vol. 302, pp. 1545–1548, Nov. 28, 2003.
[13] R. R. Johnson, A. T. C. Johnson, and M. L. Klein, "Probing the structure of DNA-carbon nanotube hybrids with molecular dynamics," *Nano Lett.*, vol. 8, pp. 69–75, 2008.
[14] C. Hu, Y. Zhang, G. Bao, Y. Zhang, M. Liu, and Z. L. Wang, "DNA functionalized single-walled carbon nanotubes for electrochemical detection," *The J. Phys. Chemistry B*, vol. 109, pp. 20072–20076, 2005.
[15] A. A. Talin, P. M. Dentinger, F. E. Jones, S. Pathak, L. Hunter, F. Leonard, and A. M. Morales, "Assembly and electrical characterization of DNA-wrapped carbon nanotube devices," *J. Vacuum Sci. Technol. B: Microelectron. Nanometer Struct.*, vol. 22, pp. 3107–3111, 2004.
[16] C. Staii, J. Alan, and T. Johnson, "DNA-decorated carbon nanotubes for chemical sensing," *Nano Lett.*, vol. 5, pp. 1774–1778, 2005.
[17] C.-L. Chen, C.-F. Yang, V. Agarwal, T. Kim, S. Sonkusale, A. Busnaina, M. Chen, and M. R. Dokmeci, "DNA-decorated carbon-nanotube-based chemical sensors on complementary metal oxide semiconductor circuitry," *Nanotechnology*, vol. 21, pp. 095504-1–095504-8, 2010.
[18] A. Paul, B. Pramanick, B. Bhattacharya, and T. K. Bhattacharyya, "DNA functionalized carbon nanotube network as humidity sensors," *IEEE Sens. J.*, vol. 13, no. 5, pp. 1806–1816, May 2013.
[19] D. Hotza and P. Greil, "Review: Aqueous tape casting of ceramic powders," *Mater. Sci. Eng. A*, vol. 202, pp. 206–217, 1995.
[20] F. Bensebaa, *Interface Science and Technology, Nanoparticle Technologies: From Lab to Market*, vol. 19, 1st ed. New York, NY, USA: Academic Press, 2012.
[21] S. Ito, P. Chen, P. Comte, M. K. Nazeeruddin, P. Liska, P. Péchy, and M. Grätzel, "Fabrication of screen-printing pastes from TiO_2 powders for dye-sensitised solar cells," *Prog. Photovolt: Res. Appl.*, vol. 15, pp. 603–612, 2007.
[22] E. J. Lavernia and N. J. Grant, "Spray deposition of metals: A review," *Mater. Sci. Eng.*, vol. 98, pp. 381–394, 1988.
[23] M. F. Mabrook, C. Pearson, and M. C. Petty, "Inkjet-printed polypyrrole thin films for vapour sensing," *Sens. Actuators B: Chem.*, vol. 115, pp. 547–551, 2006.
[24] V. Montilla, E. Ramon, and J. Carrabina, "Frequency scan technique for inkjet-printed chipless sensor tag reading," in *Proc. IEEE 17th Int. Conf. Electron., Circuits, Syst.*, Athens, Greece, 2010, pp. 1100–1103.
[25] C. Wongchoosuk, P. Jangtawee, S. Lokavee, Udomrat, P. Sudkeaw, and T. Kerdcharoen, "Novel flexible NH3 gas sensor prepared by ink-jet printing technique," *Adv. Mater. Res.*, vol. 506, pp. 39–42, 2012.
[26] N. Kamamichi, T. Maeba, M. Yamakita, and T. Mukai, "Fabrication of bucky gel actuator/sensor devices based on printing method," in *Proc. IEEE /RSJ Int. Conf. Intell. Robots Syst.*, Nice, France, Acropolis Convention Center, 2008, pp. 582–587.
[27] H. Okimoto, T. Takenobu, K. Yanagi, Y. Miyata, H. Shimotani, H. Kataura, and Y. Iwasa, "Tunable carbon nanotube thin-film transistors produced exclusively via inkjet printing," *Adv. Mater.*, vol. 22, pp. 3981–3986, 2010.
[28] J.-W. Song, J. Kim, Y.-H. Yoon, B.-S. Choi, Jae-HoKim, and C.-S. Han, "Inkjet printing of single-walled carbon nanotubes and electrical characterization of the line pattern," *Nanotechnology*, vol. 19, pp. 095702–095708, 2008.
[29] J. Spannhake, A. Helwig, O. Schulz, and G. Muller, "Micro-fabrication of gas sensors," in *In Solid State Gas Sensing*, E. Comini *et al.*, Ed. New York, NY, USA: Springer, 2009, pp. 1–46.
[30] S. J. Choi, C. Wang, C. C. Lo, P. Bennett, A. Javey, and J. Bokor, "Comparative study of solution-processed carbon nanotube network transistors," *Appl. Phys. Lett.*, vol. 101, pp. 112104–112114, 2012.
[31] K. Kordas, T. Mustonen, G. Toth, H. Jantunen, M. Lajunen, C. Soldano, S. Talapatra, S. Kar, R. Vajtai, and P. M. Ajayan, "Inkjet printing of electrically conductive patterns of carbon nanotubes," *Small*, vol. 2, pp. 1021–1025, 2006.
[32] M. Shiraishi, T. Takenobu, T. Iwai, Y. Iwasa, H. Kataura, and M. Ata, "Single-walled carbon nanotube aggregates for solution-processed field effect transistors," *Chem. Phys. Lett.*, vol. 394, pp. 110–113, 2004.
[33] P. Ferraro, S. Coppola, S. Grilli, M. Paturzo, and V. Vespini, "Dispensing nano–pico droplets and liquid patterning by pyroelectrodynamic shooting," *Nature Nanotechnol.*, vol. 5, pp. 429–435, 2010.
[34] Y. Wang, Z. Iqbal, and S. Mitra, "Rapidly functionalized, water-dispersed carbon nanotubes at high concentration," *J. Am. Chem. Soc.*, vol. 128, pp. 95–99, 2006.
[35] J. Zhao, H. Park, J. Han, and J. P. Lu, "Electronic properties of carbon nanotubes with covalent sidewall functionalization," *J. Phys. Chem. B*, vol. 108, pp. 4227–4230, 2004.
[36] A. Baba, F. Sato, N. Fukuda, H. Ushijima, and K. Yase, "Micro/nanopatterning of single-walled carbon nanotube-organic semiconductor composites," *Nanotechnology*, vol. 20, pp. 085301–085306, 2009.
[37] H. Cathcart, V. Nicolosi, J. M. Hughes, W. J. Blau, J. M. Kelly, S. J. Quinn, and J. N. Coleman, "Ordered DNA wrapping switches on luminescence in single-walled nanotube dispersions," *J. Am. Chem. Soc.*, vol. 130, pp. 12734–12744, Aug. 2008.
[38] V. Sanz, E. Borowiak, P. Lukanov, A. M. Galibert, E. Flahaut, H. M. Coley, S. R. P. Silva, and J. McFadden, "Optimising DNA binding to carbon nanotubes by non-covalent methods," *Carbon*, vol. 49, pp. 1775–1781, 2011.
[39] Y. Ono, S. Kishimoto, Y. Ohno, and T. Mizutani, "Thin film transistors using PECVD-grown carbon nanotubes," *Nanotechnology*, vol. 21, no. 20, pp. 205202-1–205202-4, 2010.
[40] N. Yamazoe and Y. Shimizu, "Humidity sensors: Principles and applications," *Sens. Actuators*, vol. 10, pp. 379–398, 1986.
[41] N. Izard, S. Kazaoui, K. Hata, T. Okazaki, T. Saito, S. Iijima, and N. Minami, "Semiconductor-enriched single wall carbon nanotube networks applied to field effect transistors," *Appl. Phys. Lett.*, vol. 92, pp. 243112-1–243112-3, 2008.
[42] Y. Zhang, K. Yua, D. Jiang, Z. Zhu, H. Genge, and L. Luo, "Zinc oxide nanorod and nanowire for humidity sensor," *Appl. Surface Sci.*, vol. 242, pp. 212–217, 2005.

Ambarish Paul received the Bachelor's (Hons.) degree in physics from Calcutta University, Kolkata, West Bengal, India, in 2004, the M.Sc. degree in physics from Banaras Hindu University, Varanasi, UP, India, in 2006, and the M.Tech. degree in advanced materials science and technology from the National Institute of Technology, Durgapur, West Bengal, India, in 2008. He is currently working toward the Ph.D. degree at the Advanced Technology Development Centre, Indian Institute of Technology Kharagpur, West Bengal, India.

His research interest includes biofunctionalization of carbon nanotube and utilizing it in sensing applications.

Baidurya Bhattacharya received the B.Tech. degree in civil engineering from the Indian Institute of Technology Kharagpur, West Bengal, India, in 1991, and the M.S. and Ph.D. degrees in civil engineering from the Johns Hopkins University, Baltimore, MD, USA, in 1994 and 1997, respectively.

He was an Assistant Professor at the University of Delaware (2001–2006) and a Visiting Faculty at Stanford University (2005) before joining the Indian Institute of Technology Kharagpur in 2006 where he became a Professor in 2011.

Tarun Kanti Bhattacharyya (M'12) received the B.Sc. degree (Hons.) in physics and the B.Tech. degree in radio-physics and electronics from the University of Calcutta, Kolkata, West Bengal, India, in 1984 and 1987, respectively, and the M.E. and Ph.D. degrees in electronics and telecommunication engineering from Jadavpur University, Kolkata, West Bengal, India, in 1991 and 1996, respectively.

He joined the Electronics and Electrical Communication Engineering Department, Indian Institute of Technology Kharagpur, West Bengal, India, in 2000 where he is currently an Associate Professor.